Journal of Power Sources 196 (2011) 2398–2402

Contents lists available at ScienceDirect

Journal of Power Sources

journal homepage: www.elsevier.com/locate/jpowsour

Short communication

Nanoporous MnO_x thin-film electrodes synthesized by electrochemical lithiation/delithiation for supercapacitors

Hui Xia, Man On Lai, Li Lu*

Department of Mechanical Engineering, National University of Singapore, 9 Engineering Drive 1, Singapore 117576, Singapore

ARTICLE INFO

Article history:
Received 8 June 2010
Received in revised form 31 August 2010
Accepted 9 September 2010
Available online 22 September 2010

Keywords:
Supercapacitor
Manganese oxide
Nanoporous
Pulsed laser deposition
Cyclic voltammetry

ABSTRACT

Nanoporous MnO_x thin-film electrodes are synthesized using a combination of pulsed laser deposition (PLD) and electrochemical lithiation/delithiation methods. A dense Mn_3O_4 thin-film deposited by PLD can transform into a nanoporous MnO_x thin-film after electrochemical lithiation/delithiation. A nanoporous MnO_x thin-film electrode exhibits significantly improved supercapacitive performance compared with an as-deposited Mn_3O_4 thin-film electrode. A MnO_x thin-film finally transforms into a MnO_2 thin-film through an electrochemical oxidation process during continuous cyclic voltammetry scanning.

1. Introduction

In recent years, great efforts have been devoted to the development of alternative energy storage/conversion devices in response to the depletion of fossil fuels and related environmental issues. Supercapacitors, as one of the important energy-storage devices, have attracted increasing attention due to their high power capability and long cycling stability [1,2]. To meet the demands for high power applications such as hybrid electric vehicles and power tools, it is important to develop advanced electrode materials with improved performance for next-generation supercapacitors.

Various materials, including active carbon [3,4], conducting polymers [5] and transition metal oxides [6,7], have been used as electrode materials for supercapacitors. Among them, transition metal oxides have been targeted due to their high specific capacitance and power. The highest specific capacitance has been reported for ruthenium oxide [8], but the high cost and toxic nature of ruthenium oxide limit its commercial application. In searching for inexpensive and alternative electrode materials, manganese oxide has been extensively investigated with the anticipation that it will replace ruthenium oxide as a low-cost and green electrode material [9–12]. One of the important strategies to improve the capacitive performance of electrode materials is to create porous structures for the electrode materials as high specific area is required for high specific capacitance and high power performance [13]. A few studies have focused on the formation of nanoporous manganese oxide [14–17]. Most synthesis strategies of nanoporous materials have been based on template-assisted methods, but these are confined by a complex synthesis process and high cost. It has been found that electrochemical lithiation/delithiation to transition metal oxide leads to in situ formation of a nanocrystalline transition metal oxide [18]. Hu et al. [19] first successfully synthesized nanoporous RuO_2 composite electrode by this method and this indicated that electrochemical lithiation/delithiation could be a room-temperature template-free method for the synthesis of nanoporous transition metal oxide. To date, however, reports on the synthesis of other nanoporous transition metal oxides by this method are still very limited. In this study, synthesis of nanoporous MnO_x thin-film electrodes by electrochemical lithiation/delithiation and their significantly improved capacitive performance are reported.

2. Experimental

Mn_3O_4 thin-films were deposited on stainless steel (SS) substrates by pulsed laser deposition (PLD) using a metallic Mn target. A Lambda Physik KrF excimer laser with wavelength 248 nm was used in the deposition. The film was deposited at a substrate temperature of 600 °C with an oxygen partial pressure of 200 mTorr. To perform the electrochemical lithiation/delithiation, a lab-made Swagelok cell was assembled with a Mn_3O_4 thin-film as the working electrode, a Li foil as both counter and reference electrode and 1 M $LiPF_6$ in EC/DEC (1/1, vol.%) as the electrolyte. The cell was charged and discharged between 0.01 and 3 V at a current

* Corresponding author. Tel.: +65 6516 2236; fax: +65 6779 1459.
E-mail addresses: mpeluli@nus.edu.sg, luli@nus.edu.sg (L. Lu).

0378-7753/$ – see front matter © 2010 Elsevier B.V. All rights reserved.
doi:10.1016/j.jpowsour.2010.09.032

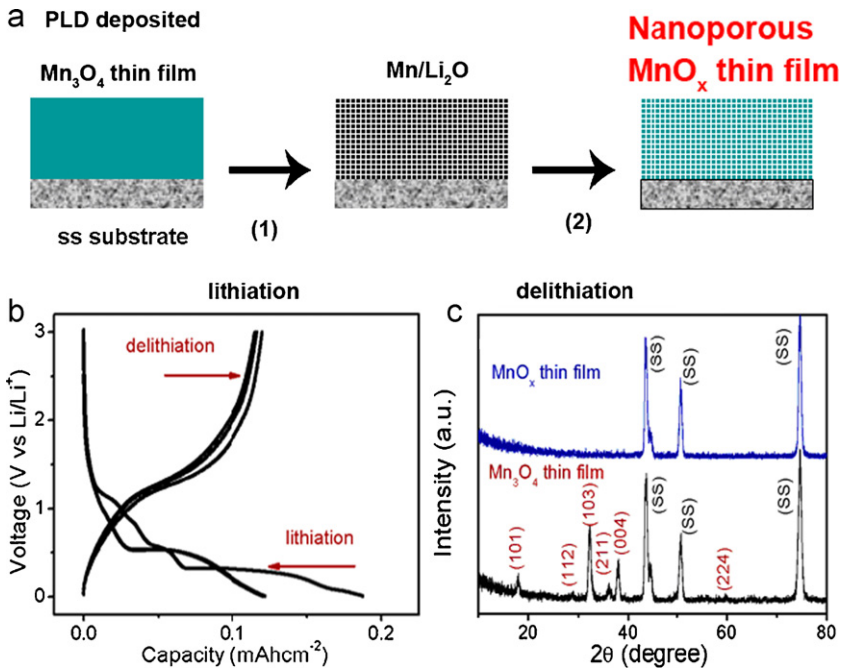

Fig. 1. (a) Schematic illustration of synthesis of nanoporous MnO_x thin-film electrode. (b) Charge–discharge curves of Mn_3O_4 thin-film electrode for electrochemical lithiation/delithiation process. (c) XRD patterns for Mn_3O_4 thin-film sample and MnO_x thin-film sample.

density of 50 μA cm^{-2} for 3 cycles. After electrochemical lithiation/delithiation, the cell was disassembled and the prepared MnO_x thin-film electrode was rinsed with deionized water, and then dried for further characterization.

The crystallographic information of the thin-film samples was investigated using powder X-ray diffraction (XRD, Shimadzu X-ray diffractormeter 6000, Cu Kα radiation). The morphologies of the Mn_3O_4 and the MnO_x thin-film samples were characterized with a field emission scanning electron microscopy (FESEM, Hitachi S4300). The morphology and structure of thin-films were further investigated by transmission electron microscopy (TEM) and high-resolution transmission electron microscopy (HRTEM, JEOL, JEM-2010). The oxidation states of Mn in the MnO_x thin-film before and after electrochemical measurement were investigated by means of X-ray photoelectron spectroscopy (XPS, PHI Quantera SXM Scanning X-ray Microprobe).

All electrochemical measurements were conducted using a Solartron 1287 electrochemical interface combined with a Solartron 1260 frequency response analyzer. For supercapacitive performance measurements, a three-electrode cell system composed of a thin-film as the working electrode, a high surface carbon rod as the counter electrode, and a Ag|AgCl reference electrode was employed. The capacitive behaviour of both the Mn_3O_4 thin-film electrode and the MnO_x thin-film electrode was characterized by cyclic voltammetry (CV) in 1 M Na_2SO_4 electrolyte at room temperature. Cyclic voltammetric measurements were performed with three-electrode cells in the voltage window between 0 and 0.9 (or 1.0) V at a scan rate of 50 mV s^{-1}. To investigate the cyclic stability of the thin-film electrode, a charge–discharge test was performed at a constant current density of 5 A g^{-1} between 0 and 1 V. Electrochemical impedance spectra (EIS) of different thin-film electrodes were measured at the open-circuit potential with an a.c. amplitude of 10 mV in the frequency range from 100 kHz to 100 mHz.

3. Results and discussion

The synthesis of the nanoporous MnO_x thin-film electrode is illustrated in Fig. 1a. First, the Mn_3O_4 thin-film is deposited on the SS substrate by PLD. Second, the Mn_3O_4 thin-film is taken through electrochemical lithiation/delithiation to make the nanoporous MnO_x thin-film. Charge–discharge curves for the electrochemical lithiation/delithiation process for the Mn_3O_4 thin-film are given in Fig. 1b. The electrochemical reaction mechanism of Li with Mn_3O_4 can be expressed by Eq. (1). During the discharge process (lithiation), Mn_3O_4 is reduced by forming a Mn/Li_2O nanocomposite in which nanometre-scale Mn clusters are embedded in a Li_2O matrix, accompanied by a large volume expansion. During the charge process (delithiation), Li is electrochemically extracted from the Mn/Li_2O nanocomposite with the formation of a nanocrystalline MnO_x thin-film electrode. As shown in Fig. 1c, before electrochemical lithiation/delithiation, the XRD spectrum of the film indicates a pure tetragonal phase of Mn_3O_4 (hausmannite). After electrochemical lithiation/delithiation, the XRD spectrum shows no diffraction peaks from the film, indicating that the film is either amorphous or nanocrystalline.

$$Mn_3O_4 + 8Li^+ + 8e^- \leftrightarrow 3Mn + 4Li_2O \quad (1)$$

Fig. 2 shows FESEM and TEM images of the as-deposited Mn_3O_4 thin-film and the MnO_x thin-film after electrochemical lithiation/delithiation. The Mn_3O_4 thin-film is composed of well-defined grains ranging from several tens to several hundreds of nanometers (Fig. 2a). Part of the film was scratched by a doctor blade for TEM characterization. A TEM image of several clustered grains from the Mn_3O_4 thin-film is given in Fig. 2b. The inserted electron diffraction (ED) pattern demonstrates the single-crystalline nature of the Mn_3O_4 grains. An SEM image of the film after the electrochemical lithiation/delithiation reveals that cracks formed in the film due to the large volume change during lithiation/delithiation (Fig. 2c). Despite the formation of cracks, no peeling of the film is observed, and this indicates that good adhesion between the film and the substrate is retained after lithiation/delithiation. In contrast to the intact single crystal grains in Fig. 2b, the grains after lithiation/delithiation are pulverized with disordered nanopores and nanograins, as shown in Fig. 2d. The HRTEM in Fig. 2e demonstrates that both nanograins and nanopores of less than 10 nm are formed. To investigate the nanoporous structure in more detail,

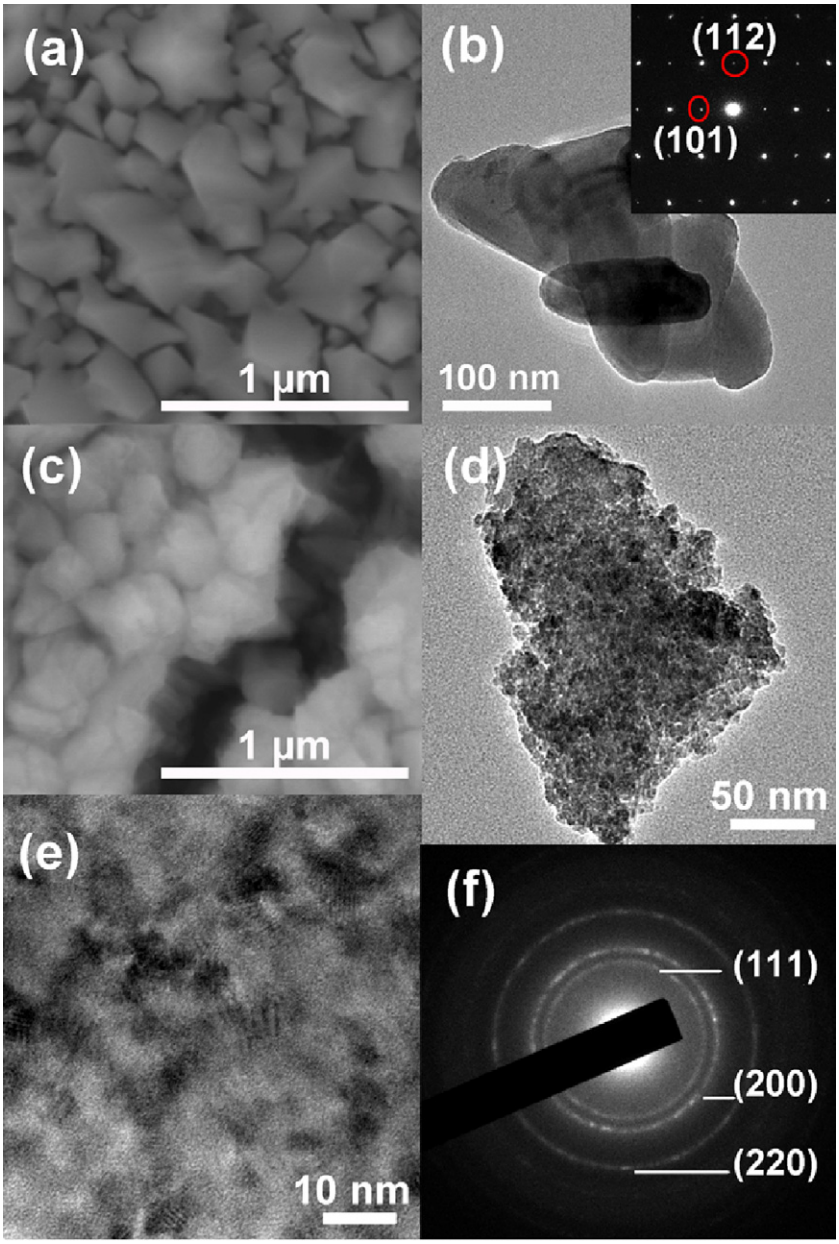

Fig. 2. (a) SEM and (b) TEM images of Mn_3O_4 thin-film sample (inset is ED pattern for Mn_3O_4 thin-film sample). (c) SEM and (d) TEM images of MnO_x thin-film sample. (e) HRTEM image of MnO_x thin-film sample. (f) ED pattern of MnO_x thin-film sample.

HRTEM images were taken from different parts of the particle (Fig. S1a), as shown in Fig. S1b–d (see Supplmentary material Fig. S1). The pore size is typically less than 10 nm for the majority of nanopores in the particle. Increasing the cycle number with repeated charge–discharge processes will probably increase the porosity or change the pore-size distribution of the film. Given the large volume change of the film during the charge–discharge processes, however, the formation of cracks is aggravated with the increasing cycle number due to the high strain, which finally leads to exfoliation of the film. Therefore, to avoid the loss of active material in the film, only three-cycle experiments were performed in this study to create the nanoporous structure. The ED pattern in Fig. 2f indicates that the original single crystalline grain becomes polycrystalline after lithiation/delithiation. Furthermore, instead of Mn_3O_4, the ED pattern can be indexed as the MnO phase. It is noticed that there is an irreversible capacity between the first discharge and charge, which indicates that not all the Li inserted in the film is removed after the delithiation process (Fig. 1b). Due to incomplete Li removal, Mn metal may not be completely oxidized to Mn_3O_4 but to MnO. It is plausible that with the gradual growth of the interphase of MnO_x during the charge process, the extraction of electrons or Li ions from the interior of the particle becomes more and more difficult due to the increased transport length. The Li extraction reaction then stops at a depth where the carriers cannot be sufficiently transported through the MnO_x phase in the timescale of the experiment, which results in a capacity loss at the first cycle. The exact composition of the film after lithiation/delithiation needs to be further investigated. Based on the ED pattern of the MnO_x thin film, it can be roughly estimated that the composition of the film is $MnO + 1/3Li_2O$. For convenience, the formula MnO_x is used to denote the film after lithiation/delithiation. To confirm that the nanoporous structure is dominant in the MnO_x thin-film, a sample was further characterized using atomic force microscopy (AFM) (see Supplementary material Fig. S2). The AFM

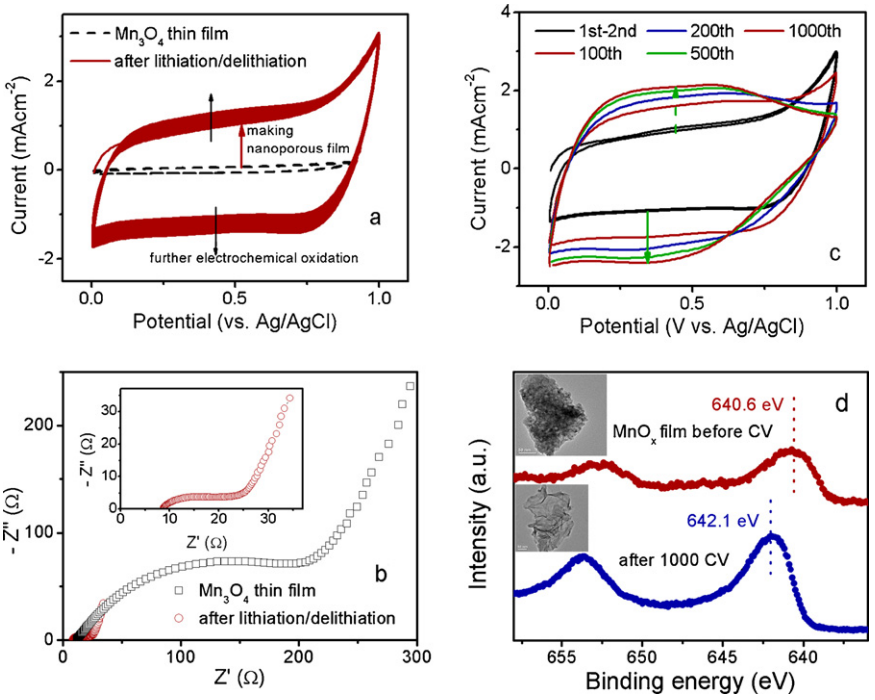

Fig. 3. (a) CV curves for Mn_3O_4 thin-film electrode and MnO_x thin-film electrode. (b) Niquist plots for Mn_3O_4 thin-film electrode and MnO_x thin-film electrode. (c) CV curves of different cycles from 1st to 1000th of MnO_x thin-film electrode. (d) Mn 2p XPS spectra for MnO_x thin-film electrode before and after 1000 CV scans (insets are TEM images of MnO_x thin-film sample before and after 1000 CV scans).

images agree well with the FESEM and TEM images, and this suggests that the nanoporous MnO_x thin-film is successfully synthesized by the electrochemical lithiation/delithiation method. As confirmed in a previous report [19], when Li is inserted into the metal oxide during the discharge process, metal nanograins are formed in a Li_2O matrix. In the present work, when the film is at the end of the discharge process, a composite with Mn nanograins in a Li_2O matrix is formed. When Li is extracted during the charge process, Mn will react with O to form MnO_x. Pore evolution is probably based on a Kirkendall-like effect between the fast-diffusion of Mn in the Mn nanograins and the relatively slow diffusion of O^{2-} ions in the Li_2O matrix, which leads to a nanograin-to-pore transition [20]. In the film, therefore, the Mn nanograins serve as templates, directing the pore formation.

Owing to its porous structure, the nanoporous MnO_x thin-film electrode is expected to exhibit superior supercapacitive performance to that of the Mn_3O_4 thin-film electrode. A comparison of the electrochemical performance between Mn_3O_4 and MnO_x thin-film electrodes is presented in Fig. 3a. The CV curve of the Mn_3O_4 thin-film electrode exhibits very low current density with a very small specific capacitance of $\sim$10 F g^{-1} due to the limited surface area. In a strong contrast, the current density of the CV curve of the nanoporous MnO_x thin-film electrode increases by nearly 20 times with a greatly improved specific capacitance of $\sim$150 F g^{-1}. Niquist plots for the Mn_3O_4 thin-film electrode and the MnO_x thin-film electrode are presented in Fig. 3b. For both Niquist plots, a semicircle in the high-frequency region and a straight line at low frequency region can be observed. The diameter of the semicircle corresponds to the charge-transfer resistance at the electrode|electrolyte interface, which is one of the limiting factors for the power density of supercapacitors [11]. It is clear that the charge-transfer resistance of the thin-film electrode reduces remarkably after electrochemical lithiation/delithiation. The small charge-transfer resistance of the MnO_x thin-film electrode is due to the formation of nanoporous structure, which facilitates the penetration of electrolyte into the electrode and greatly increases the interface area between the electrode and electrolyte. This could explain why such a significant increase in specific capacitance can be obtained after electrochemical lithiation/delithiation. EIS can also be used to estimate the electrochemical active surface area of the thin-film sample [6,21]. The electrochemical active surface area of the film can be estimated as specific value (S_a, in m^2 g^{-1}) from the double-layer capacitance (C_{dl}, in F g^{-1}, which can be obtained from EIS) of the thin-film electrode by Eq. (2):

$$S_a = \frac{C_{dl}}{C_d} \tag{2}$$

where C_d is a constant capacitance of 20 μF cm^{-2} [21,22]. Based on the double-layer capacitance C_{dl} obtained from the impedance spectrum from Fig. 3b, the electrochemical active surface area of the MnO_x thin-film is estimated to be 220 m^2 g^{-1}. It is also noticed that the current density keeps increasing with CV cycling for the MnO_x thin-film electrode, which is associated with a so-called "electrochemical activation process" corresponding to the electrochemical oxidation of low valent manganese oxide to high valent manganese oxide with potentiodynamic scans in the sodium sulfate aqueous solution [23]. The current density almost reaches a constant value after 1000 cycles, leading to a final specific capacitance of about 213 F g^{-1} (Fig. 3c). To investigate the cyclic stability of the MnO_x thin-film electrode, a test of 2000 cycles was performed at a constant current density of 5 A g^{-1} (see Supplementary material Fig. S3). It can be seen that the specific capacitance of the thin-film electrode increases significantly in the first 100 cycles and then increases slowly up to the 1000th cycle, which agrees well with the CV result as shown in Fig. 3c. The specific capacitance reaches a maximum at about the 1000th cycle and starts to decrease slowly after 1000 cycle. After 2000 cycles, the thin-film electrode still can deliver a specific capacitance of about 193 F g^{-1}, which is about 91% of the specific capacitance of the thin-film at the 1000th cycle. The Mn 2p XPS spectra for the MnO_x thin-film before and after the CV

scan are given in Fig. 3d. The peak attributed to Mn 2p3/2 shifts from 640.6 to 642.1 eV, which indicates the oxidation process from Mn^{2+} to Mn^{4+} and the formation of MnO_2 thin-film after the CV scan.

4. Conclusions

Nanoporous MnO_x thin-film electrodes have been synthesized by using electrochemical lithiation/delithiation of PLD deposited Mn_3O_4 thin-film electrodes. Nanoporous structure is formed due to reversible insertion and extraction of Li into and from the thin-film. The unique nanoporous structure of the MnO_x thin-film provides favourable paths for electrolyte penetration and high surface area for charge storage. As a result, the nanoporous MnO_x thin-film electrode exhibits remarkably enhanced specific capacitance compared with the Mn_3O_4 thin-film electrode and are therefore promising electrodes for supercapacitors. The electrochemical lithiation/delithiation synthesis procedure is simple and effective. It can also be extended to the synthesis of other nanoporous thin-films for future application in various fields such as electrochemical storage and electrocatalysis.

Acknowledgements

The research was supported by the National University of Singapore and the Agency for Science, Technology and Research through Research Grant R-265-000-292-305 (072 134 0051).

Appendix A. Supplementary data

Supplementary data associated with this article can be found, in the online version, at doi:10.1016/j.jpowsour.2010.09.032.

References

[1] H. Zhang, G.P. Cao, Y.S. Yang, Energy Environ. Sci. 2 (2009) 932.
[2] L.L. Zhang, X.S. Zhao, Chem. Soc. Rev. 38 (2009) 2520.
[3] H. Pan, C.K. Poh, Y.P. Feng, J.Y. Lin, Chem. Mater. 19 (2007) 6120.
[4] Q.T. Qu, B. Wang, L.C. Yang, Y. Shi, S. Tian, Y.P. Wu, Electrochem. Commun. 10 (2008) 1652.
[5] H.B. Zhang, H.L. Li, F.B. Zhang, J.X. Wang, Z. Wang, S.C. Wang, J. Mater. Res. 23 (2008) 2326.
[6] S.L. Chou, F.Y. Cheng, J. Chen, J. Power Sources 162 (2006) 727.
[7] G.X. Hu, C.X. Li, H. Gong, J. Power Sources 195 (2010) 6977.
[8] Y.Z. Zheng, H.Y. Ding, M.L. Zhang, Thin Solid Films 516 (2008) 7381.
[9] M.W. Xu, L.B. Kong, W.J. Zhou, H.L. Li, J. Phys. Chem. C 111 (2007) 19141.
[10] C.L. Xu, Y.Q. Zhao, G.W. Yang, F.S. Li, H.L. Li, Chem. Commun. (2009) 7575.
[11] H. Xia, W. Xiao, M.O. Lai, L. Lu, Nanoscale Res. Lett. 4 (2009) 1035.
[12] H. Xia, J.K. Feng, H.L. Wang, M.O. Lai, L. Lu, J. Power Sources 195 (2010) 4410.
[13] P. Simon, Y. Gogotsi, Nat. Mater. 7 (2008) 845.
[14] M. Nakayama, T. Kanaya, R. Inoue, Electrochem. Commun. 9 (2007) 1154.
[15] J.Y. Luo, Y.Y. Xia, J. Electrochem. Soc. 154 (2007) A987.
[16] B. Dong, T. Xue, C.L. Xu, H.L. Li, Micropor. Mesopor. Mater. 112 (2008) 627.
[17] J.Z. Zhao, Z.L. Tao, J. Liang, J. Chen, Cryst. Growth Des. 8 (2008) 2799.
[18] P. Poizot, S. Laruelle, S. Grugeon, L. Dupont, J.M. Tarascon, Nature 407 (2000) 496.
[19] Y.S. Hu, Y.G. Guo, W. Sigle, S. Hore, P. Balaya, J. Maier, Nat. Mater. 5 (2006) 713.
[20] J.W. Choi, J. McDonough, S. Jeong, J.S. Yoo, C.K. Chan, Y. Cui, Nano Lett. 10 (2010) 1409.
[21] M. Mastragostino, A. Missiroli, F. Savoi, J. Electrochem. Soc. 151 (2004) A1919.
[22] H. Shi, Electrochim. Acta 41 (1996) 1633.
[23] B. Djurfors, J.N. Broughton, M.J. Brett, D.G. Ivey, Acta Mater. 53 (2005) 957.